Biophysical Journal, Volume *114*

Supplemental Information

A Nonquiescent "Idling" Population State in Drug-Treated, *BRAF*-Mutated Melanoma

B. Bishal Paudel, Leonard A. Harris, Keisha N. Hardeman, Arwa A. Abugable, Corey E. Hayford, Darren R. Tyson, and Vito Quaranta

SUPPLEMENTARY INFORMATION FOR

A Non-Quiescent, "Idling" Population State in Drug-Treated *BRAF*-Mutated Melanoma.

B. Bishal Paudel[1,2,3], Leonard A. Harris[3,4], Keisha N. Hardeman[3,4], Arwa A. Abugable[2], Corey E. Hayford[1,3], Darren R. Tyson[3,4] and Vito Quaranta[3,4]

[1]Chemical and Physical Biology Graduate Program, [2]Vanderbilt International Scholars Program, [3]Vanderbilt Quantitative Systems Biology Center, [4]Department of Biochemistry, Vanderbilt University, Nashville, TN, USA, 37232

Address correspondence to:
Vito Quaranta
Vanderbilt University
2220 Pierce Avenue—PRB446B
Nashville, TN, 37232
Phone: (615) 936-2868 Fax: (615) 936-1190
Email: vito.quaranta@vanderbilt.edu

TABLE OF CONTENTS Page

SUPPLEMENTARY NOTE

Simple Three-State Model of Cell Proliferation

To better understand the complex dynamics exhibited by *BRAF*-mutated melanoma cells in response to *BRAF*i, including emergence of the idling phenotype, we devised a simple three-state model comprised of a regressing state *R*, a stable (zero net growth) state *S*, and an expanding state *E*. Cells in each state can experience two fates, division and death, with kinetic rate constants that are characteristic of the states. Additionally, drug induces transitions between "adjacent" states. The model can be expressed in kinetic terms as

$$Cell_R \xrightarrow{k_{gR}} Cell_R + Cell_R \quad \text{(S1)}$$

$$Cell_R \xrightarrow{k_{dR}} \emptyset \quad \text{(S2)}$$

$$Cell_S \xrightarrow{k_{gS}} Cell_S + Cell_S \quad \text{(S3)}$$

$$Cell_S \xrightarrow{k_{dS}} \emptyset \quad \text{(S4)}$$

$$Cell_E \xrightarrow{k_{gE}} Cell_E + Cell_E \quad \text{(S5)}$$

$$Cell_E \xrightarrow{k_{dE}} \emptyset \quad \text{(S6)}$$

$$Cell_R \underset{k_{sr}}{\overset{k_{rs}}{\rightleftarrows}} Cell_S \quad \text{(S7)}$$

$$Cell_S \underset{k_{es}}{\overset{k_{se}}{\rightleftarrows}} Cell_E \quad \text{(S8)}$$

Here, $Cell_X$ ($X \in \{R,S,E\}$) is the number of cells in state *X*, k_{gX} and k_{dX} are division (growth) and death rate constants for cells in state *X*, k_{XY} is the transition rate constant between states *X* and *Y* ($R \Leftrightarrow S \Leftrightarrow E$), and $\emptyset$ represents cell death (the null state). A graphical representation of the model is provided in Fig. 4A of the main text.

Given these reactions, and defining $k_{pX} \equiv k_{gX} - k_{dX}$ as the net proliferation rate for cells in state *X,* the coupled set of ordinary differential equations (ODEs) describing the state dynamics is

$$\frac{dN_R}{dt} = \left(k_{pR} - k_{rs}\right)N_R + k_{sr}N_S \quad \text{(S9)}$$

$$\frac{dN_S}{dt} = \left(k_{pS} - k_{sr} - k_{se}\right)N_S + k_{rs}N_R + k_{es}N_E \quad \text{(S10)}$$

$$\frac{dN_E}{dt} = \left(k_{pE} - k_{es}\right)N_E + k_{se}N_S \quad \text{(S11)}$$

Equations (S9)-(S11) are presented in the main text as Eqs. (1)-(3).

Model Simulation and Parameter Calibration

The model in Eqs. (S1)-(S8) consists of 10 parameters: three net proliferation rates (k_{pE}, k_{pS}, k_{pE}), four transition rate constants (k_{rs}, k_{sr}, k_{se}, k_{es}), and three initial cell counts ($N_R(t{=}0)$, $N_S(t{=}0)$, $N_E(t{=}0)$). We fixed the net proliferation rate for state *S* to zero and chose values for states *R* and *E* based on the range of responses seen for the SKMEL5 parental cell line (Fig. 2A and Fig. S4D). Specifically, we chose $k_{pR} = -0.055\,\mathrm{h}^{-1}$, $k_{pS} = 0\,\mathrm{h}^{-1}$, and $k_{pE} = 0.015\,\mathrm{h}^{-1}$. We also set the total number of initial cells T_0 = 10,000. Altogether, this eliminates four free parameters, leaving a total of six free parameters in need of calibration: the four transition rate constants and the initial *proportions* of cells in states *R* and *S* (denoted R_0 and S_0, respectively; $R_0 = N_R(t{=}0)/T_0$, etc.).

Since the drug responses across cell lines are more or less similar within the first 24h of drug addition, we assume that this is due to a delay in drug effect stabilization. We omitted this phase from model fitting. Model simulation was performed by numerically integrating Eqs. (S9)-(S11) using the LSODA algorithm (1) as implemented within the *ode* function of the R package deSolve (2). Model calibration was performed using the cost function (presented as Eq. (4) in the main text)

$$Cost = \sum_{i=1}^{n} \frac{(M_i - O_i)^2}{\sigma_i} \qquad \text{(S12)}$$

where *n* is the number of measured time points and M_i, O_i, and σ_i are the model prediction, experimentally observed value, and standard experimental error at time point *i*, respectively. We first identified the closest local minimum within the cost space using the Levenberg-Marquardt algorithm as implemented within the *modFit* function of the R package FME (3). We then performed Markov chain Monte Carlo (MCMC) sampling, using the *modMCMC* function of the FME package, to sample the trough of the cost-space well and to confirm that it was, to our best estimate, the global minimum. A Gaussian prior was defined for all parameters (4) with variances obtained from *modFit*. A lower bound of 0 was imposed for all parameters. An upper bound of 0.06/h (the observed proliferation rate for SKMEL5 cells in dimethyl sulfoxide (DMSO) control) was imposed for the transition rate constants k_{rs}, k_{sr}, k_{se}, and k_{es}. The rationale for this is based on the assumption that the transition rates have to be smaller than the maximum proliferation rates to maintain identity of the cell states (5). For the initial cell proportions R_0 and S_0, an upper bound of 1 was imposed. In addition, we required that $R_0 + S_0 \leq 1$. Constraints such as this cannot be defined directly within the *modMCMC* function. Therefore, we modified our R script to impose an artificially large cost ($>10^6$) if an MCMC iteration returned values that violated this constraint.

In all cases, we performed $1.5\text{x}10^5$ MCMC iterations ($2\text{x}10^5$ MCMC iterations performed for SKMEL28) starting from the parameter set obtained from *modFit.* Values of σ_i in Eq. (S12) were automatically determined in each case by *modMCMC* based on the input data set. The parameter covariance matrix was evaluated every 100 iterations (*updatecov* argument to *modMCMC*) and used to update the MCMC jumps. The maximum number of tries for the delayed rejection procedure was set to 2 (*ntrydr* argument to *modMCMC*). In some cases, three independent MCMC chains were run with different initial parameter values (±25% around the best fit from *modFit*) and converged to the same distributions as per the Gelman-Rubin test (6, 7). Parameter distributions for numerous cell lines are shown in Fig. S5; associated MCMC trace plots are shown in Fig. S6. In general, multi-parameter systems biology models pose a critical

challenge of parameter identifiability (8). As shown in Fig. S8, the MCMC samples of transition rate constants for SKMEL5 cells are shown as pairs plot, which shows pairwise correlations between parameters. We observed weak correlations between parameters, except for k_{sr} and k_{es}. However, we sampled parameters from parameter ensembles, and not from the individual parameter distributions to obtain our model fits and to infer epigenetic landscapes, therefore, accounting for all parameter correlations.

Three-State Discretization of Clonal Proliferation Rates

In order to compare model-generated initial cell proportions (R_0, S_0, and $E_0 = 1 - R_0 - S_0$), as determined by MCMC calibration, to experimental distributions obtained using the clonal Fraction Proliferation (cFP) assay (9) (see Fig. 4F and Fig. S4D), we had to define discrete cutoffs for the experimental data. We chose ±1 doubling every two weeks (m = ±1/360 doublings/h) for this purpose, i.e., clones doubling at a rate greater than once every two weeks are associated with the expanding state *E*, clones regressing at a rate greater than this are associated with the regressing state *R*, and clones with proliferation rates intermediate between these values are associated with the zero-net-growth state *S*. Our rationale for choosing these values is that most experiments were run over a two-week period. If a cell population did not double (or halve) over this period, then we generally considered it a slow proliferator. In Supp. Fig. 4D, we illustrate this discretization for multiple cell lines. Note that varying the cutoff values by ±10% had no qualitative effect on the conclusions of the analysis (data not shown).

Model Configurations

We additionally considered the possibility of: two-state models and three-state model with all possible phenotypic state transitions (triangle-model) in addition to our current three-state model (states organized in *linear* fashion). For the two-state models, we considered all possible combinations with: (A) Regressing (R) and Stable (S) states; (B) Stable (S) and Expanding (E) states; (C) Regressing (R) and Expanding (E) states. We also considered the three state model (*triangle* model) where the phenotypic state transitions between all states are possible. Graphical representation of all possible combinations of the models we considered is shown in Fig. S9. Phenotypic state transitions between Regressing (R) and Expanding (E) states is given by S13.

$$Cell_R \underset{k_{er}}{\overset{k_{re}}{\rightleftarrows}} Cell_E \tag{S13}$$

Given the reactions S1-S6 for proliferation kinetics of each state, phenotypic state transitions S7-8 & S13, defining $k_{pX} \equiv k_{gX} - k_{dX}$ as the net proliferation rate for cells in state *X,* the coupled set of ordinary differential equations (ODEs) describing the state dynamics in each model configurations is:

Model A

$$\frac{dN_R}{dt} = \left(k_{pR} - k_{rs}\right)N_R + k_{sr}N_S \tag{S14}$$

$$\frac{dN_S}{dt} = \left(k_{pS} - k_{sr}\right)N_S + k_{rs}N_R \tag{S15}$$

Model B

$$\frac{dN_S}{dt} = \left(k_{pS} - k_{se}\right)N_S + k_{es}N_E \tag{S16}$$

$$\frac{dN_E}{dt} = \left(k_{pE} - k_{es}\right)N_E + k_{se}N_S \quad \text{(S17)}$$

Model C

$$\frac{dN_R}{dt} = \left(k_{pR} - k_{re}\right)N_R + k_{er}N_E \quad \text{(S18)}$$

$$\frac{dN_E}{dt} = \left(k_{pE} - k_{er}\right)N_E + k_{re}N_R \quad \text{(S19)}$$

Model D

$$\frac{dN_R}{dt} = \left(k_{pR} - k_{rs} - k_{re}\right)N_R + k_{sr}N_S + k_{er}N_E \quad \text{(S20)}$$

$$\frac{dN_S}{dt} = \left(k_{pS} - k_{sr} - k_{se}\right)N_S + k_{rs}N_R + k_{es}N_E \quad \text{(S21)}$$

$$\frac{dN_E}{dt} = \left(k_{pE} - k_{es} - k_{er}\right)N_E + k_{se}N_S + k_{re}N_R \quad \text{(S22)}$$

Model E

Listed as S9-S11.

To account for all possible transitions with substantial number of cells in the starting population, we calibrated the models against an experimental time course for a 1:1:1 clonal mixture of three single cell-derived subclones (SC01, SC07, and SC10) using the Levenberg-Marquardt algorithm as implemented within the *modFit* function of the R package FME (3). We inferred the Akaike information criteria (AICc) (10, 11) for all the models we considered. Three-state model organized in linear fashion (Model E in Table S4) has the lowest AIC value and lowest residual standard error, indicating that the model E is both improved in terms of model selection and in terms of error minimization than the other possible models considered.

SUPPLEMENTARY TABLES

Table S1 | BRAF-mutated Melanoma Cell Lines

Cell Line	Stage	BRAF	P53	PTEN	NRAS	cKIT
SKMEL5	MET	V600E	WT	WT	WT	WT
A375	MET	V600E (HOMOZ)	WT	WT	WT	WT
WM793	MET	V600E	WT	Mu/HEM DEL	WT	WT
SKMEL19	MET	V600E	WT	WT	WT	WT
SKMEL28	MET	V600E (HOMOZ)	MU	MU	WT	WT
WM164	MET	V600E	MU	WT	WT	WT
WM88	MET	V600E	WT	WT	WT	WT
A2058	MET	V600E	MU	MU	WT	WT

Cell lines mutation information obtained from previously published cell databases and papers (12–15).

Table S2 | Proliferation Rates for Single Cell-Derived SKMEL5 Subclones

Proliferation rates in 8μM *BRAF*i were measured between 24-100h post drug application. Standard deviations are based on three replicates; lack of a standard deviation indicates a single measurement obtained from an initial screen.

Subclone	Prolif. rate (doublings/h)	Std. deviation
SC01	-2.13E-02	1.07E-02
SC02	4.20E-03	N/A
SC03	1.05E-02	1.48E-03
SC04	-6.51E-03	1.24E-03
SC05	9.00E-04	N/A
SC06	7.10E-03	N/A
SC07	1.53E-03	3.53E-03
SC08	-2.81E-03	3.65E-03
SC10	1.16E-02	4.16E-04
SC11	1.14E-02	N/A
SC12	1.20E-03	N/A
SC13	-2.40E-03	N/A
SC15	-1.90E-03	N/A
SC16	-2.50E-03	N/A

Table S3 | Model Variables and Parameters

Variable	Definition	
t	Time (h)	
N_R	Number of cells in state *R*	
N_S	Number of cells in state *S*	
N_E	Number of cells in state *E*	
T	Total number of cells	
Parameter	**Definition**	**Units**
k_{pR}	Net proliferation rate of cells in state *R*	h^{-1}
k_{pS}	Net proliferation rate of cells in state *S*	h^{-1}
k_{pE}	Net proliferation rate of cells in state E	h^{-1}
k_{rs}	Rate of transition of cells from state *R* to state *S*	h^{-1}
k_{sr}	Rate of transition of cells from state *S* to state *R*	h^{-1}
k_{se}	Rate of transition of cells from state *S* to state *E*	h^{-1}
k_{es}	Rate of transition of cells from state *E* to state *S*	h^{-1}
R_0	Initial proportion of cells in state *R*	unitless
S_0	Initial proportion of cells in state *S*	unitless
E_0	Initial proportion of cells in state *E*	unitless

Table S4 | Model Selection Statistics for All Model Configurations

	Model A	**Model B**	**Model C**	**Model D**	**Model E**
No. of Parameters	4	4	4	8	6
AIC value	145.6585	-363.4001	-129.4709	-394.5141	-399.7858
Residual Std. Error	1.869	0.1965	0.5533	0.1677	0.1656

SUPPLEMENTARY REFERENCES

1. Petzold, L. 1983. Automatic Selection of Methods for Solving Stiff and Nonstiff Systems of Ordinary Differential Equations. SIAM J. Sci. Stat. Comput. 4: 136–148.
2. Soetaert, K., T. Petzoldt, and R.W. Setzer. 2010. Package deSolve : Solving Initial Value Differential Equations in R. J. Stat. Softw. 33: 1–25.
3. Soetaert, K., and T. Petzoldt. 2010. Inverse Modelling , Sensitivity and Monte Carlo Analysis in R Using Package FME. J. Stat. Softw. 33: 1–28.
4. Eydgahi, H., W.W. Chen, J.L. Muhlich, D. Vitkup, J.N. Tsitsiklis, and P.K. Sorger. 2014. Properties of cell death models calibrated and compared using Bayesian approaches. Mol. Syst. Biol. 9: 644.
5. Zhou, J.X., A.O. Pisco, H. Qian, and S. Huang. 2014. Nonequilibrium population dynamics of phenotype conversion of cancer cells. PLoS One. 9.
6. Gelman, A., and D.B. Rubin. 1992. Inference from Iterative Simulation Using Multiple Sequences. Stat. Sci. 7: 457–511.
7. Brooks, S.P.B., and A.G. Gelman. 1998. General methods for monitoring convergence of iterative simulations. J. Comput. Graph. Stat. 7: 434–455.
8. Li, P., and Q.D. Vu. 2013. Identification of parameter correlations for parameter estimation in dynamic biological models. BMC Syst. Biol. 7.
9. Frick, P.L., B.B. Paudel, D.R. Tyson, and V. Quaranta. 2015. Quantifying heterogeneity and dynamics of clonal fitness in response to perturbation. J. Cell. Physiol. 230: 1403–1412.
10. Akaike, H. 1974. A new look at the statistical model identification. IEEE Trans. Autom. Control. 19: 716–723.
11. Burnham, K.P., and D.R. Anderson. 2002. Model Selection and Multimodel Inference: A Practical Information-Theoretic Approach (2nd ed). .
12. Barretina, J., G. Caponigro, N. Stransky, K. Venkatesan, A. a Margolin, S. Kim, C.J. Wilson, J. Lehár, G. V Kryukov, D. Sonkin, A. Reddy, M. Liu, L. Murray, M.F. Berger, J.E. Monahan, P. Morais, J. Meltzer, A. Korejwa, J. Jané-Valbuena, F. a Mapa, J. Thibault, E. Bric-Furlong, P. Raman, A. Shipway, I.H. Engels, J. Cheng, G.K. Yu, J. Yu, P. Aspesi, M. de Silva, K. Jagtap, M.D. Jones, L. Wang, C. Hatton, E. Palescandolo, S. Gupta, S. Mahan, C. Sougnez, R.C. Onofrio, T. Liefeld, L. MacConaill, W. Winckler, M. Reich, N. Li, J.P. Mesirov, S.B. Gabriel, G. Getz, K. Ardlie, V. Chan, V.E. Myer, B.L. Weber, J. Porter, M. Warmuth, P. Finan, J.L. Harris, M. Meyerson, T.R. Golub, M.P. Morrissey, W.R. Sellers, R. Schlegel, and L. a Garraway. 2012. The Cancer Cell Line Encyclopedia enables predictive modelling of anticancer drug sensitivity Supp. Nature. 483: 603–7.
13. Hsu, M.-Y., D.E. Elder, and M. Herlyn. 2002. Melanoma: the Wistar melanoma (WM) cell lines. In: Human cell culture. Springer. pp. 259–274.
14. Bamford, S., E. Dawson, S. Forbes, J. Clements, R. Pettett, A. Dogan, A. Flanagan, J. Teague, P.A. Futreal, M.R. Stratton, and R. Wooster. 2004. The COSMIC (Catalogue of Somatic Mutations in Cancer) database and website. Br. J. Cancer. .
15. Hardeman, K.N., C. Peng, B.B. Paudel, C.T. Meyer, T. Luong, D.R. Tyson, J.D. Young, V. Quaranta, and J.P. Fessel. 2017. Dependence On Glycolysis Sensitizes BRAF-mutated Melanomas For Increased Response To Targeted BRAF Inhibition. Sci. Rep. 7: 42604.

SUPPLEMENTARY FIGURES

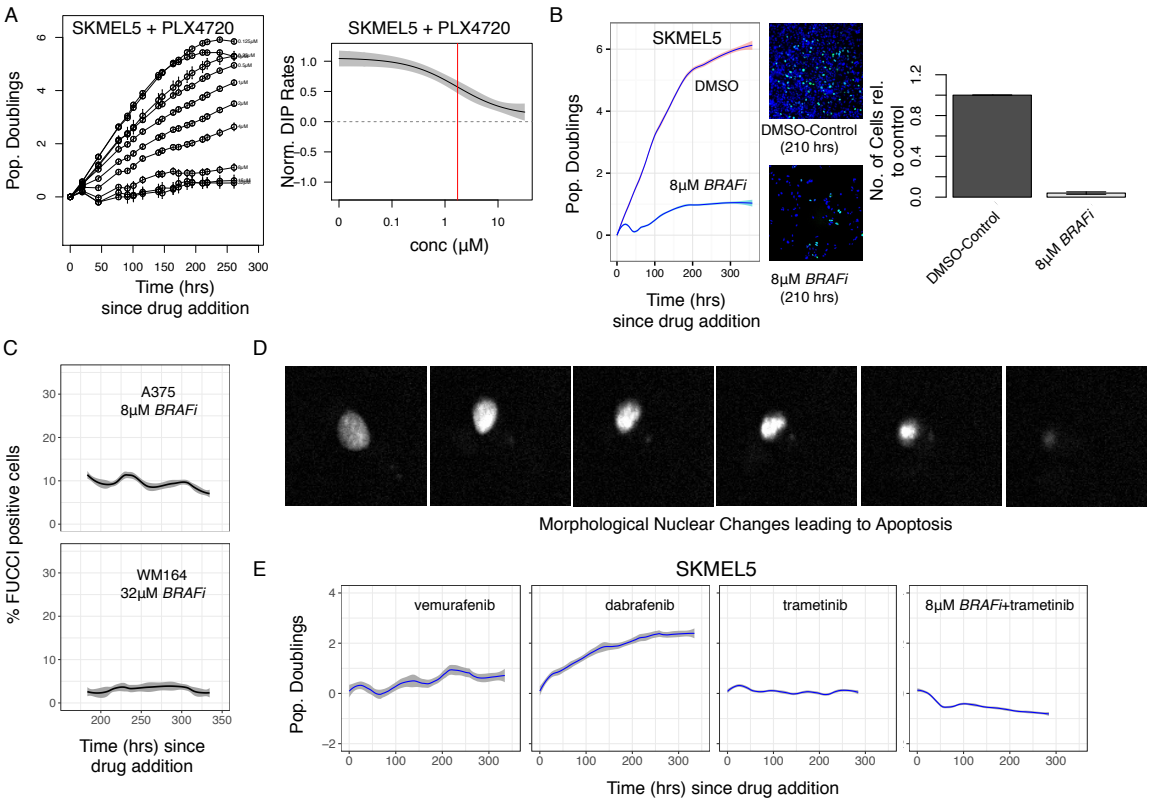

Figure S1: *BRAF*i-Induced Responses of *BRAF*-Mutated Melanoma Cell Populations. (a) *(left)* Population growth curves (log2 normalized) for SKMEL5 parental cells treated with varying concentrations of *BRAF*i; *(right)* DIP rate-based dose–response curve (red line is the EC_{50}). (b) The idling state is not trivially due to confluence: (*left*) comparison of population growth curves (log2 normalized) for SKMEL5 cells treated with *BRAF*i and DMSO control; (*right*) representative images at 210 h post *BRAF*i treatment (nuclei are shown in blue, FUCCI-positive (cycling) cells in green). (c) Percentage of FUCCI-positive cells for A375 and WM164 cells between 168-350h of treatment with 8 μM *BRAF*i and 32 μM *BRAF*i respectively. (d) Nuclear morphological changes leading to apoptosis observed in *BRAF*i-treated SKMEL5 cells. (e) Population growth curves (log2 normalized) for SKMEL5 parental cells treated with 16 μM vemurafenib, 4 μM dabrafenib, 0.125 μM trametinib, and a combination of 8 μM *BRAF*i and 0.125 μM trametinib *(*mean responses are shown as solid lines, 95% confidence intervals as shaded regions).

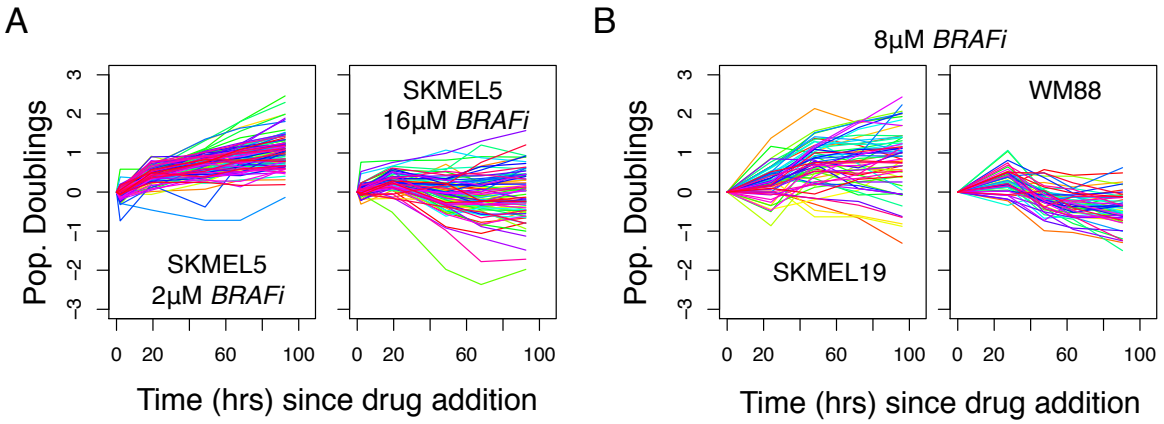

Figure S2: Clonal Responses of Multiple *BRAF*-mutated Melanoma Cell Lines to Various Concentrations of *BRAF*i (a) Population growth curves (log2 normalized) obtained using the cFP assay for SKMEL5 single cell-derived colonies treated with 2 μM *BRAF*i (n=106) and 16μM *BRAF*i (n=95). (b) Population growth curves (log2 normalized) obtained using the cFP assay for single cell-derived colonies of SKMEL19 (n=60) and WM88 (n=55) treated with 8 μM *BRAF*i.

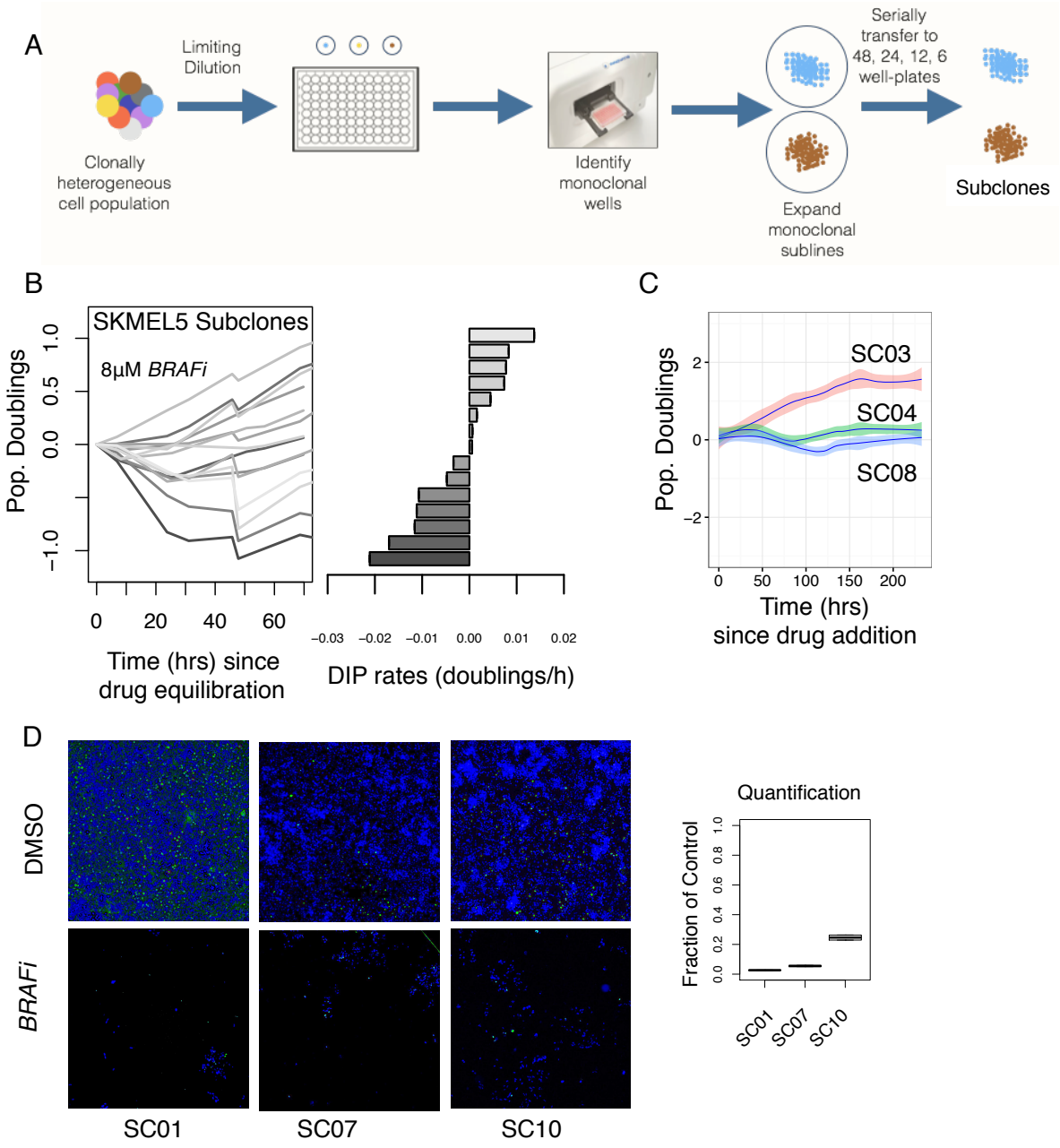

Figure S3: Responses of Single Cell-Derived SKMEL5 Subclones Treated with *BRAF*i (a) Schematic of single-cell-cloning technique used to isolate single cell-derived subclones. (b) 16 single cell-derived SKMEL5 subclones treated with 8 μM *BRAF*i: (*left*) population growth curves (log2 normalized); (*right*) bar-plot of *BRAF*i-treated sub clone DIP rates calculated as linear fits to the growth curves. (c) Three additional SKMEL5 single cell-derived subclones (SC03, SC04, SC08) idle after prolonged exposure to *BRAF*i. (d) (*left*) Representative images at 190 h post drug addition of populations of SKMEL5 subclones SC01, SC07, and SC10 in DMSO and treated with *BRAF*i; (*right*) cell fractions in *BRAF*i relative to DMSO control.

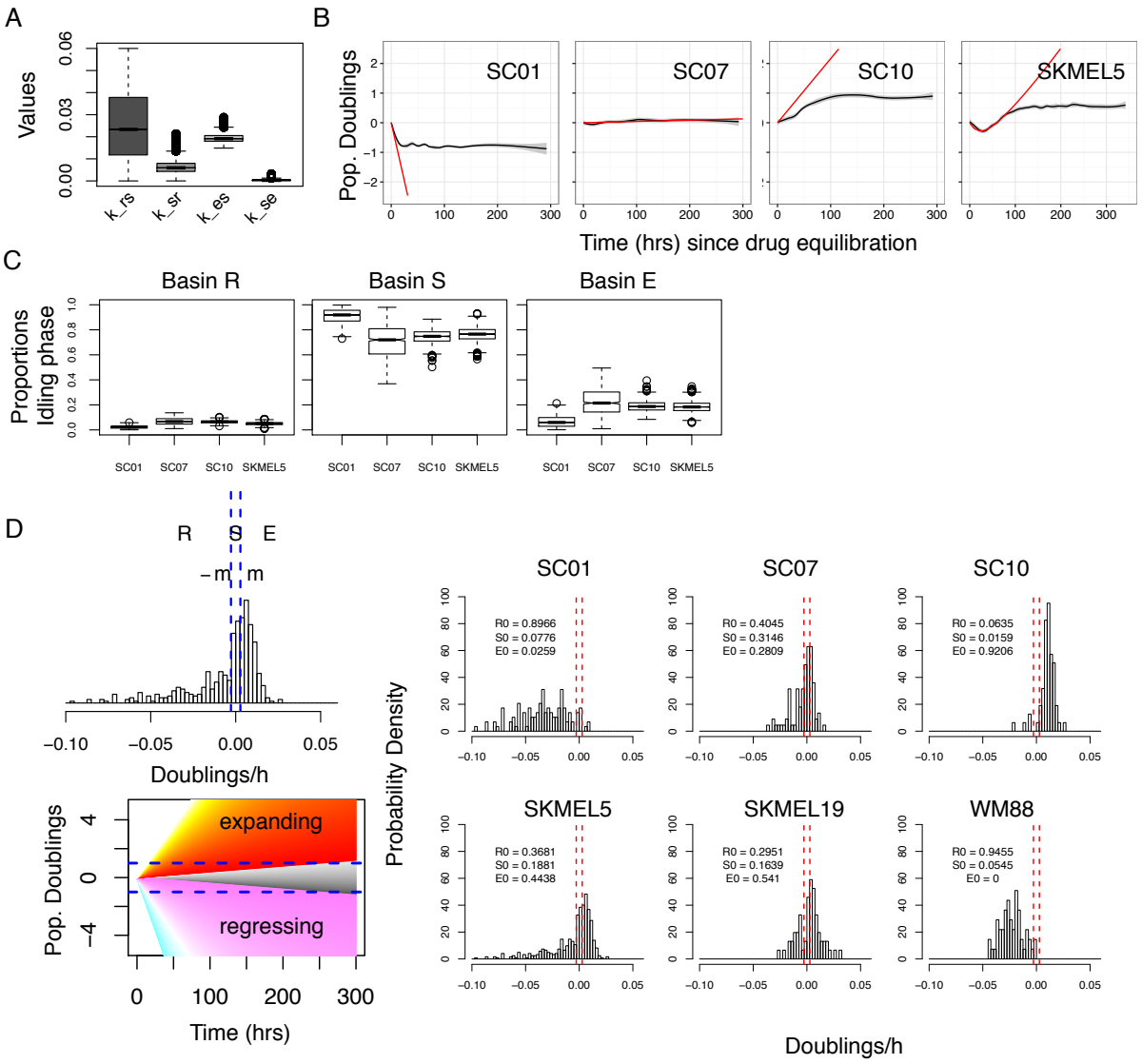

Figure S4: Model Predictions and State Discretization for Multiple BRAF-mutated Melanoma Cell Lines and Subclones (a) Distributions of transition rate constants (k_{rs}, k_{sr}, k_{se}, k_{es}) obtained by MCMC calibration of our three-state model to experimental data for a 1:1:1 clonal mixture of subclones SC01, SC07, and SC10 (boxes extend from the first to third quartile, solid horizontal line is the median, whiskers extend to 1.5x the interquartile range, outliers are shown as empty circles). (b) Experimental population growth curves (black solid line with 95% confidence envelope) for SKMEL5 parental and single cell-derived subclones SC01, SC07, and SC10 overlaid with model predictions (red) if all transition rate constants are set to zero. (c) Model-predicted proportions of cells in the regressing (*R*), stationary (*S*), and expanding (*E*) subpopulations in the idling state for SKMEL5 parental and single cell-derived subclones SC01, SC07, SC10. (d) Discretizing cFP distributions into three states: (*left*) Cutoffs (+/- m) of one doubling every two weeks (+/-1/360 doublings/h) defines the regressing state *R*, the zero-net-growth state *S*, and the expanding state *E*; (*right*) cFP distributions for multiple *BRAF*i-treated melanoma cell lines with quantified cell state proportions.

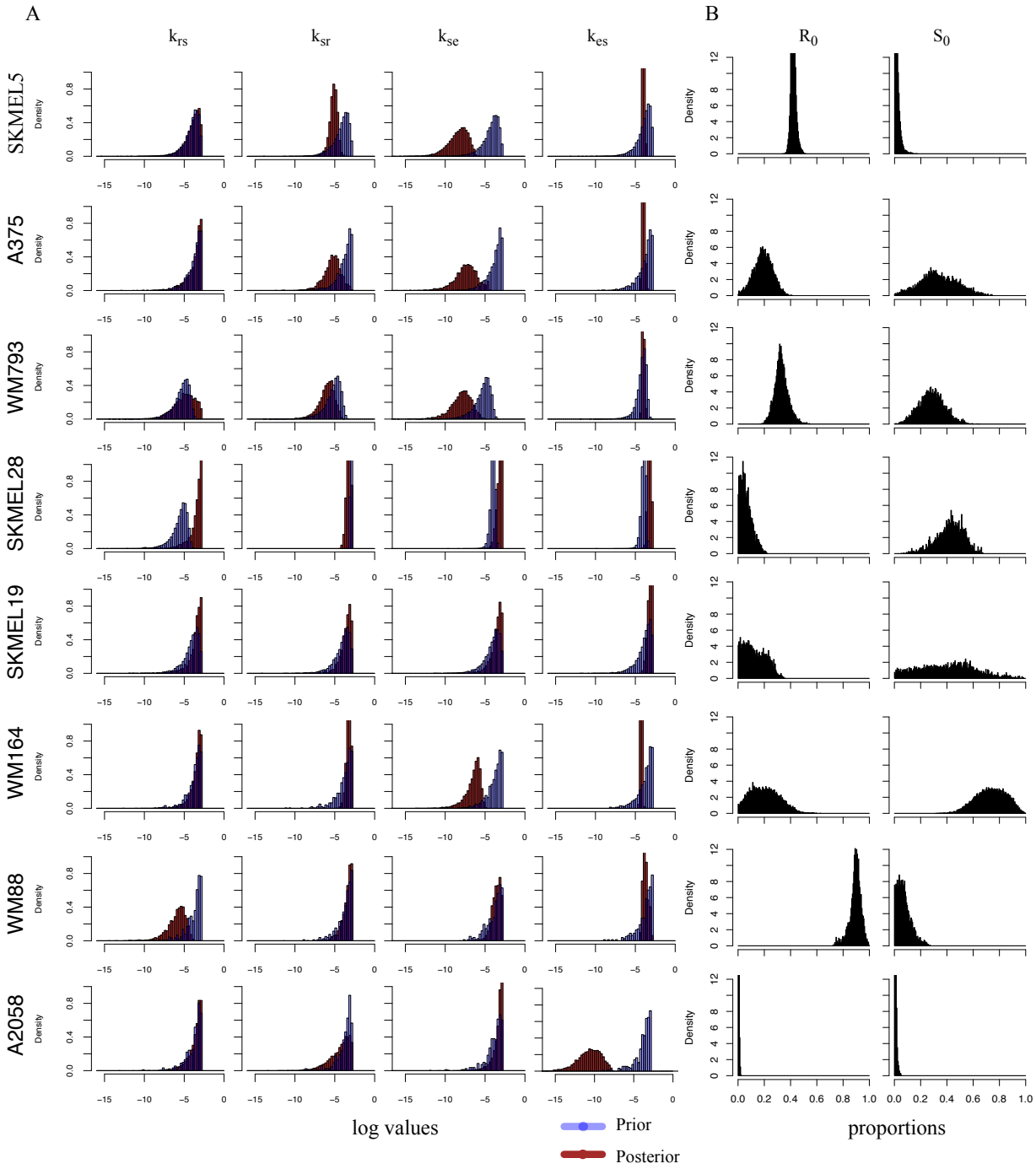

Figure S5: Parameter Distributions Obtained by MCMC Calibration Against Experimental Data for Multiple *BRAF*-mutated Melanoma Cell Lines. (a) Transition rate constants (log scale); depicted in blue are the prior distributions while depicted in red are posterior distributions. (b) Proportions of initial cells counts.

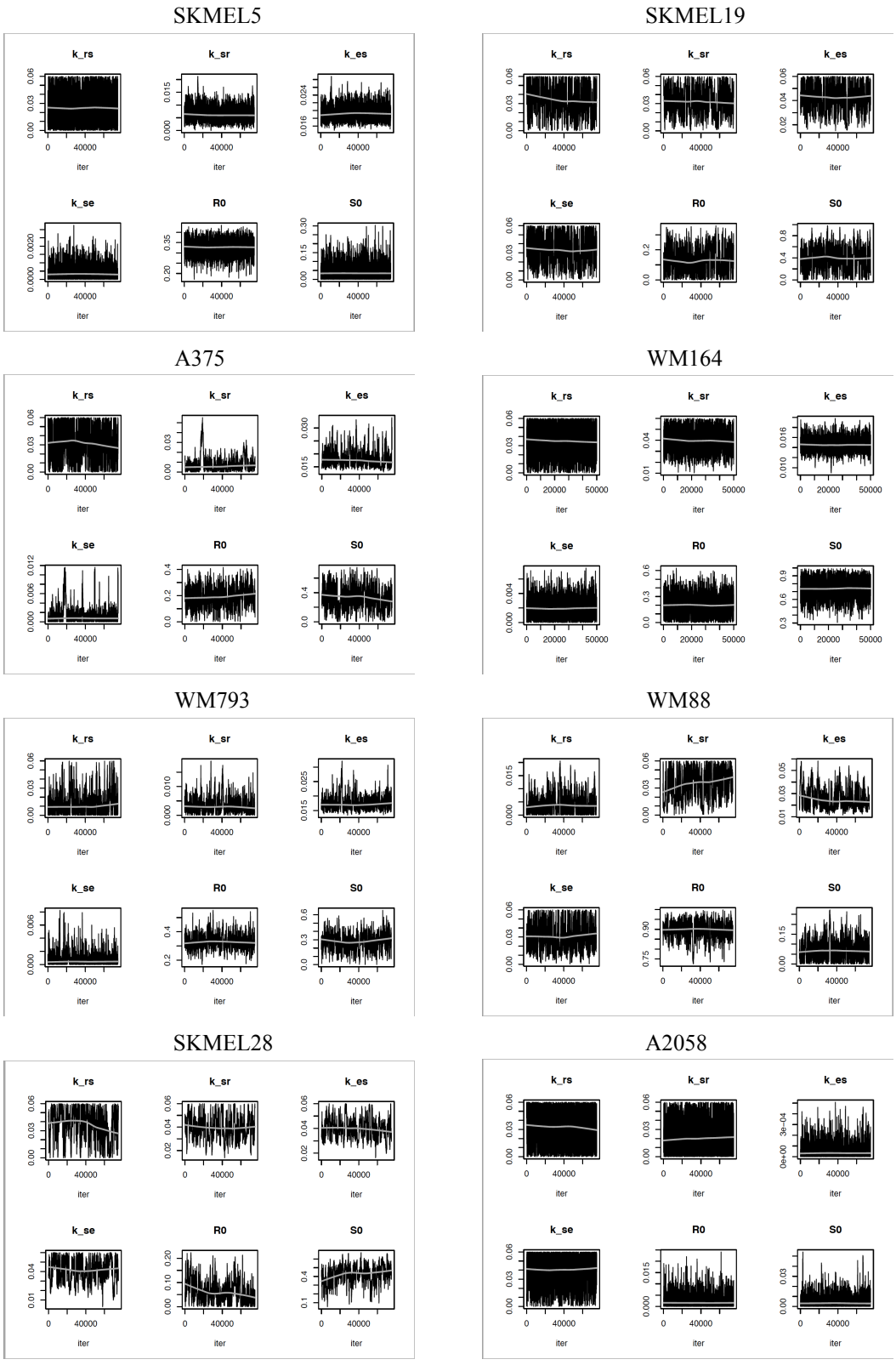

Figure S6: MCMC Trace Plots for Multiple *BRAF*-mutated Melanoma Cell Lines. The last 50% (accounting for burn-in) of the 1.5x10^5 total MCMC iterations are shown.

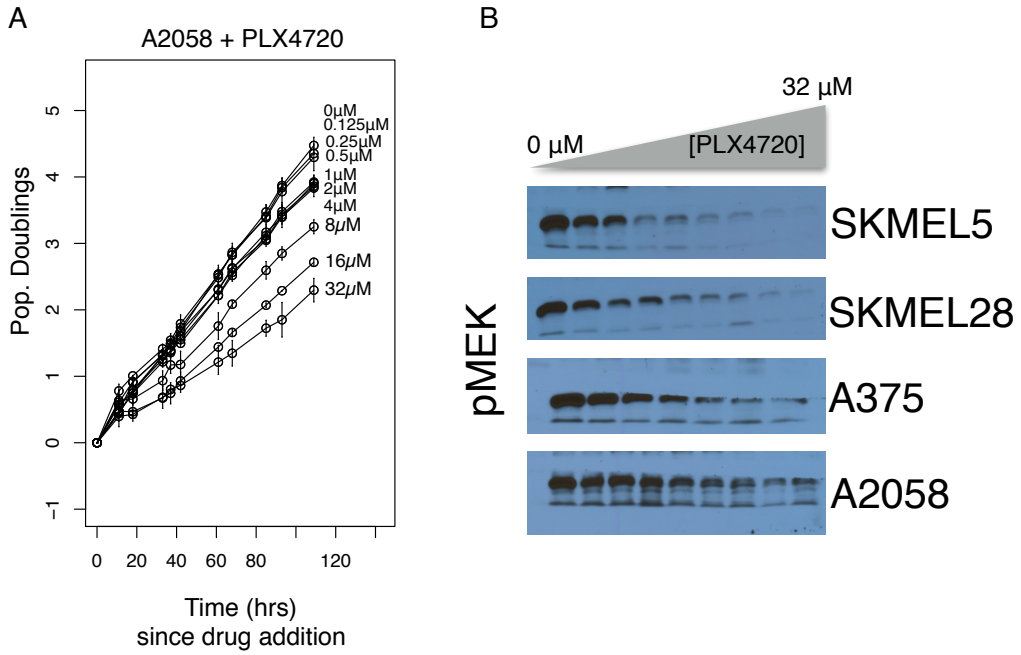

Figure S7: *BRAF*i-Induced Population Dynamics and Signaling Changes for the A2058 Cell Line. (a) Population growth curves (log2 normalized) for varying concentrations of *BRAF*i. (b) Western blots comparing levels of phosphorylated MEK in A2058 cells and three other cell lines after 96h exposure to *BRAF*i (lanes correspond to drug concentrations in for the population growth curves).

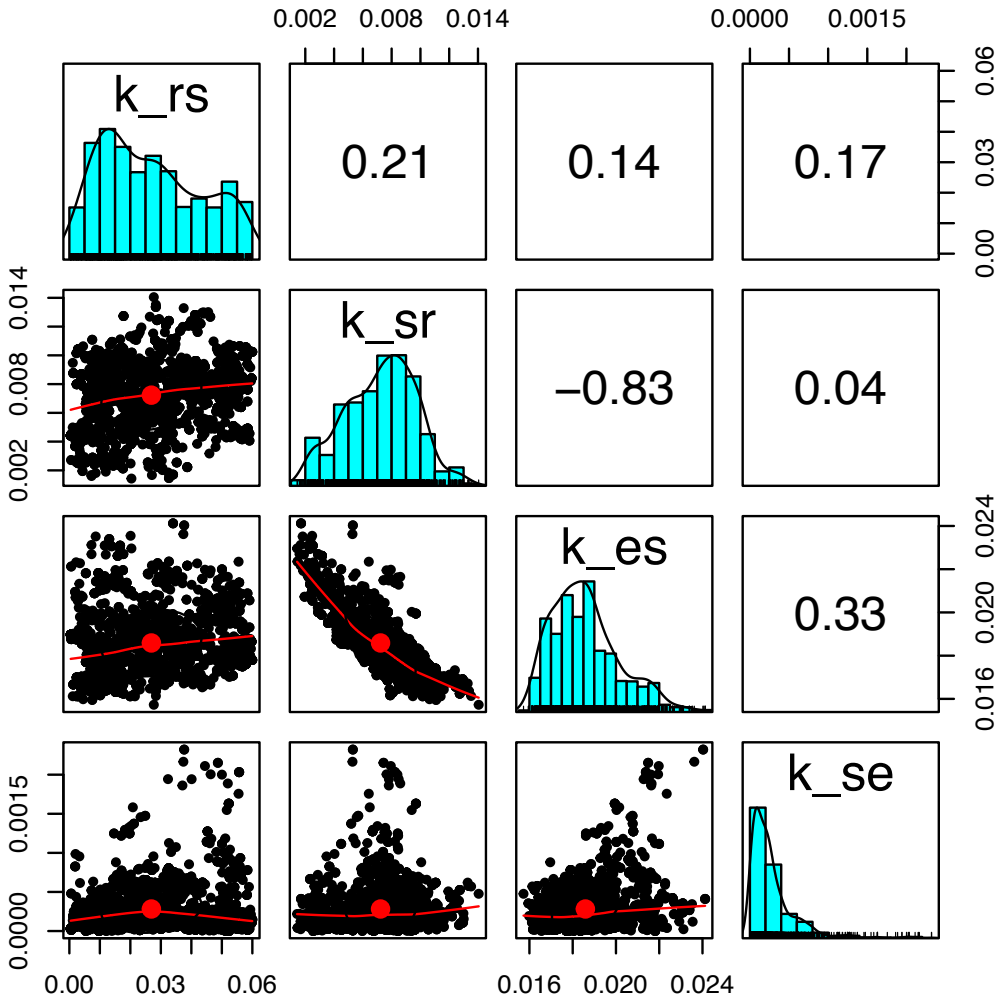

Figure S8: Correlations Between Transition Rate Constants Obtained by MCMC Calibration. (a) Pairs plot of the Markov Chain Monte Carlo samples for the transition rate constants of SKMEL5 cells. The pairwise relationship is in the bottom plot, the correlation coefficient is in the top plot, and distribution of each parameter is on the diagonal.

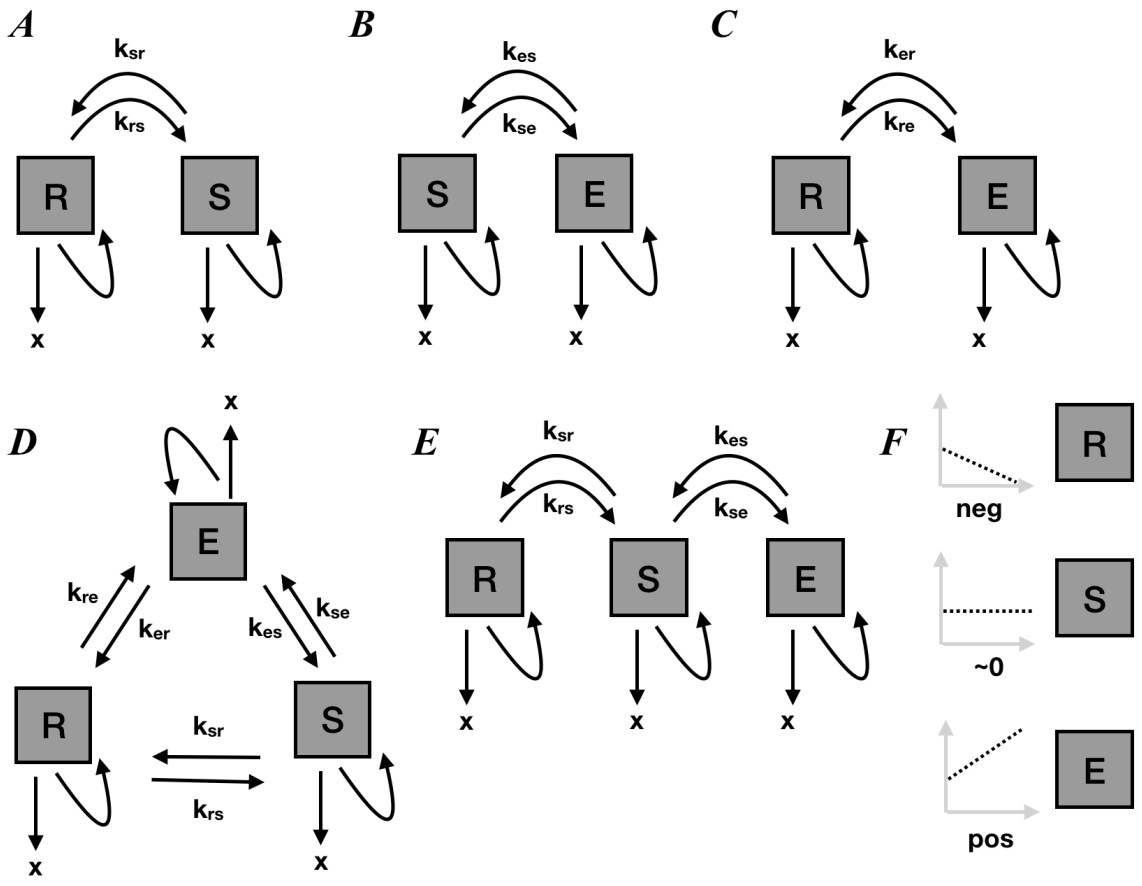

Figure S9: Graphical Representation of All Possible Model Configurations Considered. Two-state models with: (a) Regressing (R) and Stationary (S) states; (B) Stationary (S) and Expanding (E) states; (C) Regressing (R) and Expanding (E) states; (D) Three-state model with all possible state transition among states, also called "triangle" model; (E) Three-state model organized in linear fashion. (F) Population dynamics of the proposed three-states. In all the states, cells can divide, die or transition into another available states.